Letter

Hilbert space fragmentation and interaction-induced localization in the extended Fermi-Hubbard model

Philipp Frey [1,*] Lucas Hackl [2,1,†] and Stephan Rachel [1,‡]
[1]*School of Physics, The University of Melbourne, Parkville, Victoria 3010, Australia*
[2]*School of Mathematics and Statistics, The University of Melbourne, Parkville, Victoria 3010, Australia*

(Received 7 October 2022; accepted 15 November 2022; published 2 December 2022)

We study Hilbert space fragmentation in the extended Fermi-Hubbard model with nearest- and next-nearest-neighbor interactions. Using a generalized spin/mover picture and saddle point methods, we derive lower bounds for the scaling of the number of frozen states and for the size of the largest block preserved under the dynamics. We find fragmentation for strong nearest- and next-nearest-neighbor repulsions as well as for the combined case. Our results suggest that the involvement of next-nearest-neighbor repulsions leads to an increased tendency for localization. We then model the dynamics for larger systems using Markov simulations to test these findings and unveil in which interaction regimes the dynamics becomes spatially localized. In particular, we show that for strong nearest- and next-nearest-neighbor interactions random initial states will localize provided that the density of initial movers is sufficiently low.

DOI: 10.1103/PhysRevB.106.L220301

Dynamical thermalization and ergodicity breaking in closed many-body quantum systems have been subjects of renewed interest in recent years. Advances in controlled experimental and quantum simulation techniques have allowed us to observe quantum dynamics with unprecedented resolution and even to engineer entirely novel many-body Hamiltonians [1–9]. This experimental progress is accompanied by new theoretical insights into the emergence of thermodynamic properties from quantum dynamics. In addition, possible exceptions to what seems to be the generic mechanism of thermalization have been under investigation in recent years [10–18]. A thermal Hamiltonian is characterized by eigenstates that look thermal with respect to local observables and have additional properties that ensure that arbitrary initial states thermalize, as long as they are not unphysical. These properties are summarized in what is called the *eigenstate thermalization hypothesis* (ETH) [17,19,20]. One of the proposed exceptions to ETH is many-body localization, which can be understood as an emergent integrability caused by local quenched disorder [11,14,21–26]. A different mechanism is quantum many-body scars [27–34]. These are a set of eigenstates of measure zero in the thermodynamic limit that violate ETH. A third mechanism of ergodicity breaking, that of *Hilbert space fragmentation*, describes the phenomenon that local constraints can separate the Hilbert space into exponentially many subspaces that are spanned by product states and are dynamically disconnected from each other [34–42]. The Hamiltonian assumes a block-diagonal structure with respect to a product basis, and the number of blocks is exponential in system size L. This results in a small number of accessible states and can prevent a typical initial product state from thermalizing. One may distinguish strong and weak fragmentation by comparing the dimension $\mathcal{D}_{\max}$ of the largest block to the dimension $\mathcal{D}$ of the entire Hilbert space. The former is characterized by $\mathcal{D}_{\max}/\mathcal{D} \to 0$; the latter is characterized by $\mathcal{D}_{\max}/\mathcal{D} \to 1$ as $L \to \infty$. One striking feature of fragmentation is the abundance of so-called *frozen states*, i.e., local product states that are also eigenstates of the Hamiltonian and hence evolve trivially. The most prominent class of systems that have been shown to be fragmented are dipole moment-conserving models in which only local multiparticle hopping terms are present [34,38,40,41]. The nature of these constraints can lead to spatial localization of the dynamics in the sense that the occupancy of certain sites remains fixed over time [35]. This is accompanied by a transition from weak to strong fragmentation. Another route to fragmentation relies on interaction-induced local constraints [43,44]. It was shown that the integrable spinless Fermi-Hubbard chain features a fragmented Hilbert space in the infinite interaction strength limit [44].

In this Letter, we extend the spinless Hubbard model by adding a next-nearest-neighbor term and consider various limits and their effect on Hilbert space fragmentation and localization. Making use of a convenient mapping of product states onto symbol strings, we derive effective hopping rules for the novel cases. They lead us to construct frozen states as well as large Hilbert space blocks. Classical Markov simulations allow us to explore spatial localization in said limits beyond system sizes that can be diagonalized exactly [35]. The effective rules are particularly simple for only nearest-neighbor constraints and combined nearest- and next-nearest-neighbor constraints. While the former case is clearly delocalized, our findings suggest that the additional next-nearest-neighbor interactions induce localization.

*pfrey@student.unimelb.edu.au
†lucas.hackl@unimelb.edu.au
‡stephan.rachel@unimelb.edu.au

Extended Fermi-Hubbard model. We consider the t-V_1-V_2 spinless fermionic chain with periodic boundary conditions (PBCs) imposed,

$$\hat{H} = -t\sum_x (\hat{c}^\dagger_{x+1}\hat{c}_x + \text{H.c.}) + V_1 \sum_x \hat{n}_x\hat{n}_{x+1} + V_2 \sum_x \hat{n}_x\hat{n}_{x+2}. \tag{1}$$

$\hat{c}_x$ creates an electron on site x, and t is the hopping amplitude. V_1 and V_2 denote nearest- and next-nearest-neighbor repulsion, respectively. We note that the model is integrable (nonintegrable) for $V_2 = 0$ ($V_2 \neq 0$). Hamiltonian (1) has been studied as a genuine fermionic model but also in its closely related hard-core boson form [45–47] as an anisotropic spin-$\frac{1}{2}$ XXZ chain [48,49] and the six-vertex model of statistical mechanics [50]. The important limit $V_1 \to \infty$ and $V_2 = 0$ was explicitly worked out for fermions using a spin/mover picture in [43]. Both limits ($V_1 \to \infty, V_2 = 0$) and ($V_2 \to \infty, V_2 = 0$) lead to a locally constrained hopping term:

$$\hat{H}^{(1,2)}_\infty = -\sum_x \hat{P}^{(1,2)}_x (\hat{c}^\dagger_{x+1}\hat{c}_x + \text{H.c.}) \hat{P}^{(1,2)}_x, \tag{2}$$

with the local projectors $\hat{P}^{(1)}_x = 1 - (\hat{n}_{x+2} - \hat{n}_{x-1})^2$, which projects onto states where $\hat{n}_{x-1} = \hat{n}_{x+2}$, and $\hat{P}^{(2)}_x = 1 + \frac{1}{4}[(\hat{n}_{x-2} + \hat{n}_{x+2} - \hat{n}_{x-1} - \hat{n}_{x+3})^4 - 5(\hat{n}_{x-2} + \hat{n}_{x+2} - \hat{n}_{x-1} - \hat{n}_{x+3})^2]$, which projects onto states with $n_{x-2} + n_{x+2} = n_{x-1} + n_{x+3}$, respectively.

In the limit $V_1 \to \infty$ and $V_2 \to \infty$, both constrains act simultaneously [51]:

$$\hat{H}^{(3)}_\infty = -\sum_x \hat{P}^{(2)}_x \hat{P}^{(1)}_x (\hat{c}^\dagger_{x+1}\hat{c}_x + \text{H.c.}) \hat{P}^{(1)}_x \hat{P}^{(2)}_x. \tag{3}$$

Note that $\hat{P}^{(1)}_x$ and $\hat{P}^{(2)}_x$ commute.

There are three relevant operators that are preserved in certain limits, namely, the total number of particles $\hat{N} = \sum_x \hat{c}^\dagger_x\hat{c}_x$; the number of *bonds* $\hat{N}^{(1)}_{\bullet\bullet} = \sum_x \hat{n}_x\hat{n}_{x+1}$, i.e., lattice bonds with both of the adjacent sites occupied; and the number of second-order bonds $\hat{N}^{(2)}_{\bullet\bullet} = \sum_x \hat{n}_x\hat{n}_{x+2}$.

The Hamiltonian always conserves N, which allows us to focus on the half-filling sector ($N = \frac{L}{2}$) with dimension

$$\mathcal{D}_{\text{half}} = \binom{L}{\frac{L}{2}} \sim \sqrt{\frac{2}{L\pi}}\, 2^L. \tag{4}$$

In contrast, $N^{(1)}_{\bullet\bullet}$ is conserved only in the limit $V_1 \to \infty$, and $N^{(2)}_{\bullet\bullet}$ is conserved in the limit $V_2 \to \infty$. Thus, the Hilbert space of $\hat{H}^{(i)}_\infty$ fragments into disjoint blocks of product states characterized by their filling N and respective bond numbers $N^{(1)}_{\bullet\bullet}$ and/or $N^{(2)}_{\bullet\bullet}$. As derived in the Supplemental Material [52] (part A), for a chain of L sites the largest symmetry sector is characterized by $N = \frac{L}{2}$ and, depending on which quantities are conserved, $N^{(1)}_{\bullet\bullet} = \frac{L}{4}$ and/or $N^{(2)}_{\bullet\bullet} = \frac{L}{4}$. The dimension of these symmetry sectors scales with the dimension of the full Hilbert space, i.e., 2^L, multiplied by some polynomial correction (see the Supplemental Material [52], part A, and Table I).

Mapping to spins and movers. It turns out that even within each symmetry sector there is further fragmentation due to the local constraints on particle hopping. In particular, *frozen states* are product states that are simultaneously eigenstates of $\hat{H}^{(i)}_\infty$, so they correspond to one-dimensional blocks of $\hat{H}^{(i)}_\infty$.

TABLE I. We consider the half-filling sector $N = \frac{L}{2}$ and list the lower bounds $\mathcal{D}_{\text{frozen}}$, for the number of frozen states in this sector, and $\mathcal{D}_{\text{max}}$, for the dimension of the largest block in this sector. We compare them to $\mathcal{D}_{\text{sym}}$, which is the dimension of the largest symmetry sector, i.e., $N^{(1)}_{\bullet\bullet} = \frac{L}{4}$ for $V_1 \to \infty$, $N^{(2)}_{\bullet\bullet} = \frac{L}{4}$ for $V_2 \to \infty$, and both combined for $V_1, V_2 \to \infty$. While they symbol $\sim$ indicates exact asymptotics, the symbol $\gtrsim$ indicates only a lower bound for the asymptotics.

	$\mathcal{D}_{\text{frozen}}$	$\mathcal{D}_{\text{max}}$	$\mathcal{D}_{\text{sym}}$
$V_1 \to \infty$	$\sim \frac{0.74}{\sqrt{L}}(1.62)^L$	$\sim 0.11\sqrt{L}\,(1.61)^L$	$\sim \frac{1.27}{L} 2^L$
$V_2 \to \infty$	$\gtrsim \frac{4.98}{L}(1.22)^L$	$\gtrsim \frac{2.26}{\sqrt{L}}(1.50)^L$	$\sim \frac{1.27}{L} 2^L$
$V_1, V_2 \to \infty$	$\gtrsim \frac{0.74}{\sqrt{L}}(1.62)^L$	$\gtrsim \frac{1.13}{\sqrt{L}}(1.41)^L$	$\sim \frac{2.03}{L^{3/2}} 2^L$

Let us illustrate this for $\hat{H}^{(1)}_\infty$ with $L = 8, N = 4$, and $N^{(1)}_{\bullet\bullet} = 2$. Indicating filled (empty) by $\bullet$ ($\circ$), the state $|\bullet\bullet\circ\circ\bullet\bullet\circ\circ\rangle$ is frozen, as it is an eigenstate. Spatial translations generate four such states in total. One may use these states as a starting point to construct further blocks of states by shifting particles in a systematic fashion. The state $|\bullet\bullet\bullet\circ\circ\bullet\circ\circ\rangle$, for example, is in the same symmetry sector but is clearly dynamically disconnected from any frozen state. The single particle on the right can hop freely until it encounters the block of three particles on the left, in which case it can assist in the hopping of said particles, i.e.,

$$\begin{aligned}|\bullet\bullet\bullet\circ\circ\bullet\circ\circ\rangle &\to |\bullet\bullet\bullet\circ\bullet\circ\circ\circ\rangle \to |\bullet\bullet\circ\bullet\bullet\circ\circ\circ\rangle \\ &\to |\bullet\circ\bullet\bullet\bullet\circ\circ\circ\rangle \to |\circ\circ\bullet\bullet\bullet\circ\circ\bullet\rangle \to \cdots . \end{aligned} \tag{5}$$

The free particle is called a *mover* for obvious reasons, and the above example illustrates that a mover passing through the entire chain results in a state that is shifted by two sites with respect to the initial state; that is, in this case we would not have localization.

In order to analyze the Hilbert space fragmentation in the limits $V_1 \to \infty$ and $V_2 \to \infty$, it is useful to map the states from the *occupation number picture* to a *spin/mover* picture [43,44]. For this, we adopt the following rules: Every bond $\bullet\bullet$ is assigned an up spin $\uparrow$, and every pair of unoccupied sites $\circ\circ$ is assigned a down spin $\downarrow$. Furthermore, we introduce so-called *movers* $\mathbf{0}$ associated with alternating sequences, e.g., $\bullet\circ\bullet$, $\circ\bullet\circ$, $\bullet\circ\bullet\circ$, $\circ\bullet\circ\bullet$, etc., of length n, which is mapped to $\lfloor\frac{n-1}{2}\rfloor$ movers.

This mapping can be compactly summarized as

$$|\underbrace{\bullet\bullet\cdots\bullet\bullet}_{n_1}\overbrace{\circ\bullet\cdots\circ\bullet}^{n_2}\underbrace{\circ\circ\cdots\circ\circ}_{n_3}\rangle \equiv |\underbrace{\uparrow\cdots\uparrow}_{n_1-1}\underbrace{\mathbf{0}\cdots\mathbf{0}}_{\lfloor\frac{n_2-1}{2}\rfloor}\underbrace{\downarrow\cdots\downarrow}_{n_3-1}\rangle, \tag{6}$$

where we illustrate two blocks of spins separated by a block of movers. Note that our counting of the mover sequences (length of alternating sequence) is such that the last and first sites also count towards the spin blocks [see overlapping braces in (6)]. For periodic boundary conditions the mapping to spin/movers is not injective, as sometimes two quantum states are mapped to the same spin/mover states (see the Supplemental Material [52], part B).

Effective dynamics. In order to analyze fragmentation and localization in each of the three limits $\hat{H}^{(1,2,3)}_\infty$, we employ the general strategy of deriving effective hopping rules in the

spin-mover picture. Using these rules, we systematically construct frozen states and large blocks and derive the asymptotic scaling of their number and dimension, respectively. In the case of $\hat{H}_\infty^{(1)}$ the effective rules are especially simple, and it is clear that any product state but a frozen state dynamically delocalizes. The cases $\hat{H}_\infty^{(2,3)}$ require a more detailed analysis. We use statistical arguments and numerical evidence to show that the dynamics of $\hat{H}_\infty^{(2)}$ is also delocalized, while $\hat{H}_\infty^{(3)}$ is typically localized. However, introducing the average mover density as a control parameter gives rise to a transition between localized and delocalized dynamics in $\hat{H}_\infty^{(3)}$.

Fragmentation for $V_1 \to \infty$. We introduce the number of spin ups $N_\uparrow$, the number of spin downs $N_\downarrow$, the number of movers N_0, and the number of times the pattern $\downarrow\uparrow$ appears in the spin sequence $N_{\downarrow\uparrow}$. Then we find the following constraints: $N_\uparrow = N_\downarrow = \frac{N}{2}$ and $N_{\downarrow\uparrow} + N_0 = N_{\bullet\bullet}^{(1)}$. Every state corresponds to a sequence of $\uparrow$, $\downarrow$, and $\mathbf{0}$'s, and the constrained dynamics corresponds to the $\mathbf{0}$'s moving freely through the sequence with the additional condition that moving every $\mathbf{0}$ through the entire chain results in a cyclic permutation of the spin sequence (PBCs imposed), i.e.,

$$\begin{aligned}|\uparrow\uparrow\downarrow\mathbf{0}\downarrow\rangle &\to |\uparrow\uparrow\mathbf{0}\downarrow\downarrow\rangle \to |\uparrow\mathbf{0}\uparrow\downarrow\downarrow\rangle \\ &\to |\mathbf{0}\uparrow\uparrow\downarrow\downarrow\rangle \to |\downarrow\uparrow\uparrow\downarrow\downarrow\mathbf{0}\rangle \to \ldots, \end{aligned} \tag{7}$$

which corresponds to (5) rewritten in spins. The dimension $\mathcal{D}_{\text{frozen}}$ of the frozen state block for $V_1 \to \infty$ and half filling can be computed analytically. For this, we recall that for $\hat{H}_\infty^{(1)}$ only the movers can move, so a state is frozen if it does not contain any movers, i.e., there are no $\mathbf{0}$'s in the spin picture. We can organize such frozen states by the number $2w$ of spin domains (up and down spins). For L sites and $2w$ domains, there must be $\frac{L}{2} - w$ spins of each type, which we need to distribute over the different domains. Using the saddle point method reviewed in the Supplemental Material [52] (part C1), we find the asymptotics

$$\mathcal{D}_{\text{frozen}} \sim \sqrt{\tfrac{3\sqrt{5}-5}{\pi L}}\left(\tfrac{1+\sqrt{5}}{2}\right)^L = \frac{0.74}{\sqrt{L}}(1.62)^L. \tag{8}$$

The number of frozen states is exponentially suppressed in the sector of half filling with $\mathcal{D}_{\text{half}} = \binom{L}{\frac{L}{2}} \sim \sqrt{\frac{2}{\pi L}}\, 2^L$. While their dynamics is trivially localized, a generic initial state will thus not have sufficient overlap with frozen states to make its dynamics also local.

The largest block for $V_1 \to \infty$ is found in [44] using the spin/mover picture. It corresponds to states with $N_0 = \frac{L}{4} - 1$ movers (corresponding to $\frac{L}{2}$ sites) that move freely through two regions (one filled, one empty) of $\frac{L}{4}$ sites each, i.e., generated by

$$|\bullet\circ\cdots\bullet\circ\bullet\bullet\cdots\bullet\bullet\circ\circ\cdots\circ\circ\rangle = |\mathbf{0}\cdots\mathbf{0}\uparrow\ldots\uparrow\downarrow\ldots\downarrow\rangle\,. \tag{9}$$

Starting with the spin state $|\uparrow\ldots\uparrow\downarrow\ldots\downarrow\rangle$, we can cyclically rotate the spins to get $\frac{L}{2}$ different states, which can then be filled by distributing the N_0 movers over the $\frac{L}{2}$ positions between the spins. We therefore count a block dimension of

$$\mathcal{D}_{\max} = \tfrac{L}{2}\binom{\frac{L}{2}+N_0-1}{N_0} \sim \sqrt{\frac{L}{27\pi}}\left(\frac{3^{3/4}}{\sqrt{2}}\right)^L = 0.11\sqrt{L}(1.61)^L. \tag{10}$$

Hopping rules:

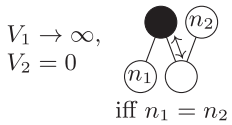

(1) Free movement:
$|\cdots\updownarrow\mathbf{0}\cdots\rangle \leftrightarrow |\cdots\mathbf{0}\updownarrow\cdots\rangle$

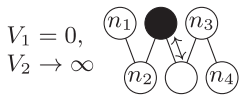

(2a) Creation/annihilation:
$|\cdots\uparrow\uparrow\downarrow\downarrow\cdots\rangle \leftrightarrow |\cdots\uparrow\mathbf{0}\downarrow\cdots\rangle$
$|\cdots\downarrow\downarrow\uparrow\uparrow\cdots\rangle \leftrightarrow |\cdots\downarrow\mathbf{0}\uparrow\cdots\rangle$

(2b) Constrained movement:
$|\cdots S_1\mathbf{0}\updownarrow S_2\cdots\rangle \leftrightarrow |\cdots S_1\updownarrow\mathbf{0}\,S_2\cdots\rangle$
iff $S_1 = S_2 = \updownarrow$ or $S_1 \neq \updownarrow \neq S_2$

FIG. 1. We illustrate the spin mapping, which allows us to map the fermionic Fock states to a sequence of spins $\downarrow\uparrow$ and so-called *movers* $\mathbf{0}$ based on [43]. Movers move freely and are preserved in $\hat{H}_\infty^{(1)}$, while in $\hat{H}_\infty^{(2)}$ they are constrained and can be created/annihilated based on the illustrated rules. For $V_1, V_2 \to \infty$, we have only the constrained movement (2b). The symbol $\updownarrow$ represents a spin that is fixed to either up or down.

We have $\lim_{L\to\infty} \frac{\mathcal{D}_{\max}}{\mathcal{D}_{\text{sym}}} = 0$, where $\mathcal{D}_{\text{sym}}$ is the dimension of the relevant symmetry sector (see Supplemental Material [52], part A), so $\hat{H}_\infty^{(1)}$ admits strong Hilbert space fragmentation. At the same time, we see explicitly that the movers $\mathbf{0}$ can move freely through the whole system. As this applies to all blocks, except frozen states, $\hat{H}_\infty^{(1)}$ will not show any localization for generic initial states.

Fragmentation for $V_2 \to \infty$. In order to simplify the dynamics and to bring similar combinatorial arguments to bear on this problem, we use the same mapping as before, i.e., every state is now written as a sequence of $\uparrow$, $\downarrow$, and $\mathbf{0}$'s. However, the hopping rules are now given by rules (2a) and (2b) in Fig. 1, where $\updownarrow$ represents either an up or down spin and $S_{1,2} \in \{\uparrow, \downarrow, \mathbf{0}\}$ can be any symbol. We see that it is still the movers ($\mathbf{0}$'s) that hop, although with further constraints. However, the number of movers is no longer conserved since they can be created and annihilated by certain spin configurations.

Note that rule (2a) leads to a second-order hopping process for movers in certain configurations, e.g.,

$$|\cdots\uparrow\mathbf{0}\downarrow\uparrow\uparrow\cdots\rangle \leftrightarrow |\cdots\uparrow\uparrow\downarrow\downarrow\uparrow\uparrow\cdots\rangle \leftrightarrow |\cdots\uparrow\uparrow\downarrow\mathbf{0}\uparrow\cdots\rangle\,. \tag{11}$$

Since the model is symmetric under a global transformation $n_x \leftrightarrow 1 - n_x$, there is a corresponding hopping process when globally substituting $\uparrow \leftrightarrow \downarrow$. Hence, we see that movers can trade position with antialigned spins if the pattern is framed by identical spins that are aligned with the outer spin of the antialigned pair. as illustrated in (11).

In the Supplemental Material [52] (part C2), we systematically construct frozen states as spin configurations that cannot generate movers and derive a lower asymptotic bound $\mathcal{D}_{\text{frozen}}$ for the number of frozen states, namely.

$$\mathcal{D}_{\text{frozen}} \gtrsim \frac{4.98}{L}\,(1.22)^L. \tag{12}$$

By comparison with numerical results, it is clear that these spin states do not contribute the bulk of frozen

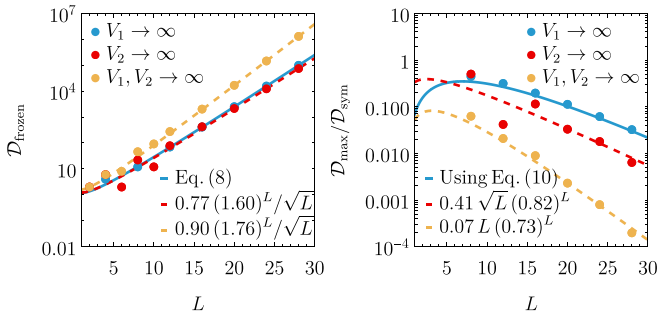

FIG. 2. Analysis of $\mathcal{D}_{\text{frozen}}$ and $\mathcal{D}_{\text{max}}/\mathcal{D}_{\text{sym}}$ by comparing the exact values with our analytics ($V_1 \to \infty$) and numerical fits ($V_2 \to \infty$, $V_1, V_2 \to \infty$), confirming $\mathcal{D}_{\text{max}}/\mathcal{D}_{\text{sym}} \to 0$ as $L \to \infty$ (strong fragmentation). Here, $\mathcal{D}_{\text{max}}$ refers to the largest Block within the largest symmetry sector, whose dimension is $\mathcal{D}_{\text{sym}}$ (see Table I).

states for $V_2 \to \infty$. Instead, states containing frozen movers represent the majority of such states in the asymptotic limit.

In the Supplemental Material [52] (part C3), we construct a lower bound $\mathcal{D}^{-}_{\text{max}}$ for the dimension of the largest block as some involved sum over binomial factors. We then expand the summand for large L, convert the sum into an integral, and then extract the asymptotics using the saddle point method to find

$$\mathcal{D}_{\text{max}} \gtrsim \frac{4}{\sqrt{\pi L}}\sqrt[4]{5}^{L} \approx \frac{2.26}{\sqrt{L}}(1.50)^{L}. \tag{13}$$

Fragmentation for $V_1, V_2 \to \infty$. The case where both interactions terms are taken *independently* to infinity, i.e., $V_1 \to \infty$ and $V_2 \to \infty$, is characterized by the conservation of $\hat{N}$, $\hat{N}^{(1)}_{\bullet\bullet}$, and $\hat{N}^{(2)}_{\bullet\bullet}$. Therefore, rule (2b) from Fig. 1 describes the only allowed hopping for movers.

All frozen states in the limit $V_1 \to \infty$ are also frozen in the limit $V_1, V_2 \to \infty$, so we immediately find the previously derived asymptotics (8) for $V_1 \to \infty$ as a lower bound, i.e.,

$$\mathcal{D}_{\text{frozen}} \gtrsim \sqrt{\tfrac{3\sqrt{5}-5}{\pi L}}\left(\tfrac{1+\sqrt{5}}{2}\right)^{L} = \frac{0.74}{\sqrt{L}}(1.62)^{L}. \tag{14}$$

From Fig. 2, we see that this already describes the asymptotics well, but a numerical fit indicates that the leading coefficient should be around 2.59 instead of 0.74. We thus see that even in the limit $V_1, V_2 \to \infty$ the frozen block still represents a fraction $\mathcal{D}_{\text{frozen}}/\mathcal{D}_{\text{half}} \to 0$ that vanishes exponentially fast, so that we need to focus on the larger blocks to analyze potential localization.

For the construction of large blocks the same starting point can be used as in the case $V_2 \to \infty$ since the contribution from states with $n = 2\lceil \frac{L}{8} \rceil$ and $N_{\mathbf{0}} = \frac{L}{2} - 2\lceil \frac{L}{8} \rceil$ makes use of only rule (2b). We therefore find the lower bound on the dimension $\mathcal{D}_{\text{max}}$ of the largest block to be

$$\mathcal{D}_{\text{max}} \geqslant \binom{n+N_{\mathbf{0}}}{N_{\mathbf{0}}} \sim \tfrac{4^n}{\sqrt{\pi n}} = \tfrac{\sqrt{2}^L}{\sqrt{\pi L/4}} \approx \tfrac{1.13}{\sqrt{L}}(1.41)^{L}. \tag{15}$$

The problem of localization. Our key findings are summarized in Table I and Fig. 2, where we study the dimensions of the frozen state space $\mathcal{D}_{\text{frozen}}$ and of the largest block $\mathcal{D}_{\text{max}}$ within the half-filling sector. We find in all three limits $V_1 \to \infty, V_2 \to \infty$, and $V_1, V_2 \to \infty$ that the frozen states are exponentially suppressed ($\mathcal{D}_{\text{frozen}}/\mathcal{D}_{\text{half}} \sim e^{-\alpha L}$) and hence should not cause typical states to stay localized. We then study larger blocks and determine the dimension scaling of the largest block $\mathcal{D}_{\text{max}}$. While we find freely moving **0**'s in the states of large blocks and thus delocalized dynamics, we also see that for $V_2 \to \infty$ and $V_1, V_2 \to \infty$ there exist Hamiltonian blocks generated from states where individual movers are constrained due to barriers that do not let movers pass through according to rule (2b) from Fig. 1. Thus, we conclude that $V_1 \to \infty$ does not lead to localization, while the limits $V_2 \to \infty$ and $V_1, V_2 \to \infty$ require a more detailed analysis.

We have seen that the limit $V_1 \to \infty$ yields fragmentation, while the dynamics is not localized in real space (with the exception of frozen states). We may attribute the existence of large blocks to the fact that each mover is spatially unconstrained, so a finite number of movers contributes a binomial coefficient to the dimension of the block generated by such states. We were able to construct large blocks in the limit $V_2 \to \infty$ by carefully choosing a generating state that allows for fully delocalized dynamics despite the restricted hopping rule (2b). This begs the question of whether full spatial delocalization is typical even for the cases $V_2 \to \infty$ and $V_1, V_2 \to \infty$. We will analyze this question using classical Markov simulations [35].

Markov simulations for $V_2 \to \infty$. We consider random states with a fixed density of movers n_0. We do this by first generating strings of spin and mover symbols of length m and a total of $n_0 m$ movers. We subsequently convert these to states in real space characterized by their local occupancies. These states are then time evolved via a Markov simulation (see the Supplemental Material [52], part D), during which we keep track of active sites, i.e., those sites that change their occupancy at any point in the simulation. We find that essentially, all initial states result in a fully delocalized dynamics, except for very low densities n_0, as one might expect from the fact that large blocks are prevalent for $V_2 \to \infty$. We can explain this fact by showing explicitly that typical states should delocalize based on rules (2a) and (2b). The problem can be broken down into two parts. First, consider random strings of spins with no movers. Rule (2a) will generate a mover for any $\uparrow\uparrow\downarrow\downarrow$ / $\downarrow\downarrow\uparrow\uparrow$ pattern within the string. These occur with a rate $r = \frac{N_{\uparrow\uparrow\downarrow\downarrow}}{m} = 1/8$ and should follow a Poisson distribution. Therefore, the distance between two consecutive patterns of this type should be Poisson distributed with mean $\mu = 1/r = 8$. Applying rule (2a) will reduce the number of symbols between the resulting movers by two, and we find that the symbol distance Δ between movers is a shifted Poisson distribution. We are left with a string of random spins that does not contain any $\uparrow\uparrow\downarrow\downarrow$ / $\downarrow\downarrow\uparrow\uparrow$ patterns and a finite number of movers embedded within it. Second, we consider one such mover and its surrounding spins and study the size of the active region generated by it. It is clear that any activity has to spread locally from this single mover in a random spin background. We perform Markov simulations on random symbol strings of this type. For a given number m of spin symbols to the right of the central mover we identify the site in real space that corresponds to the end of

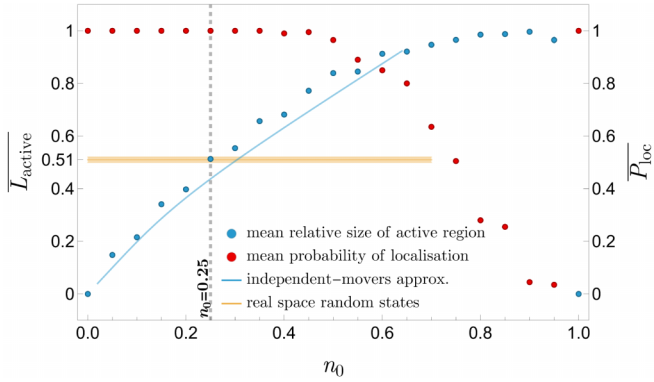

FIG. 3. For $V_1, V_2 \to \infty$, we show the mean size of the active regions $\overline{L_{\text{active}}}$ relative to the total system size for random symbol strings with $M_{\text{total}} = 31$ symbols and $n_0 M_{\text{total}}$ movers in blue. The solid blue line corresponds to the predicted value of $\overline{L_{\text{active}}}$ based on an independent-mover model. We show the mean active size for random states in real space with fixed length $L_{\text{total}} = 42$ in solid orange and the mean probability of localization $\overline{P_{\text{loc}}}$ as a function of mover density for random symbol strings with $M_{\text{total}} = 31$ in red. The dotted gray line marks the intersection of blue and solid orange lines and hence indicates that real-space random states correspond to a mover density $n_0 = 0.25$. All Markov simulations use 400 random initial strings and 8×10^4 time steps each.

the mth symbol and keep track of its activity. This allows us to sample the cumulative probability distribution [CDF(m)] of activity over a range of symbols $0 \leqslant m \leqslant 15$ (see Fig. 3 in the Supplemental Material [52]). We find that the distribution saturates at a value of $\text{CDF}_{\max} \approx 0.53$ at $m \approx 5$, indicating that in around half of all cases the active region is confined to fewer than five symbols and otherwise spreads indefinitely due to an avalanche effect. We can now find the probability that two consecutive movers produce active regions that do *not* connect:

$$\mathcal{P}_{\text{disc}} = \sum_{\Delta} \mathcal{P}_{\text{sep}}(\Delta) \sum_{m=0}^{\Delta-1} \text{CDF}(m)\ \text{PDF}(\Delta - m) \approx 0.26. \tag{16}$$

Here, P_{sep} is the distribution of distance between consecutive movers, and PDF is the probability density function associated with the cumulative distribution CDF. The avalanche effect implies that essentially, every active region associated with a mover has to remain finite in order to avoid full delocalization and therefore the probability of localization for a random symbol string of length m is $\mathcal{P}_{\text{loc}} \approx (\text{CDF}_{\max})^{mr}$. Adding additional movers by setting $n_0 > 0$ will affect $\mathcal{P}_{\text{sep}}$ and hence lower the value of $\mathcal{P}_{\text{disc}}$. However, its main effect on the probability of localization is via a shift in the exponent: $\mathcal{P}_{\text{loc}}^{(n_0)} \approx (\text{CDF}_{\max})^{m(r+n_0)}$. This explains why only very low initial mover densities n_0 and short chains yield a significant fraction of localized states.

Markov simulations for $V_1, V_2 \to \infty$. This case is characterized by only rule (2b), and the treatment in terms of active and inactive regions can be done analytically. A mover in a random spin background can hop past a given spin with probability $p = \frac{1}{2}$ according to (2b). Hence, the probability of creating an active region that extends over m spins is

$$P_{\text{S}}(m) = \sum_{n=0}^{m} p^n p^{n-m} (1-p)^2 = (m+1)\, 2^{-(m+2)}. \tag{17}$$

The mean free path of a mover is given by $\overline{m} = \sum_m m P_{\text{S}}(m) = 2$. Numerically, we find a compatible distribution in the real-space length L using a Markov simulation with $t = 10^5$ time steps and a sample of 1000 initial symbol strings if we account for the relation $L \approx 1.65m$.

In order to estimate the size of active regions as a function of mover density we make the ansatz

$$\frac{M_{\text{active}}}{M_{\text{total}}} = \frac{L_{\text{active}}}{L_{\text{total}}} = n_0(\overline{m} - \bar{x}), \tag{18}$$

where M_{active} and L_{active} are the number of active sites in symbol space and real space, respectively. Likewise, M_{total} and L_{total} are the total numbers of symbols and sites, respectively. $\bar{x}$ is the average overlap between neighboring active regions. We estimate $\bar{x}$ assuming that neighboring active regions are dynamically independent, which turns out to be a good approximation for not too large mover densities.

Figure 3 shows data obtained from Markov simulations along with a prediction based on the independent-mover approximation. The latter fails to be accurate above $n_0 \approx 0.7$, where we numerically find essentially no dependence on n_0. The probability of localization, defined as a nonvanishing number of inactive sites, is essentially $P_{\text{loc}} = 1$ up to $n_0 \approx 0.5$. Comparing the mean size of active regions for random states in real space, i.e., equal probability of occupancy 0 or 1 on each site, with that of random states in symbol space of fixed mover density, we find that the mean mover density of the former is $\overline{n_0} = 0.25$. Therefore, random states in real space are well within the localized regime, and the limit $V_1, V_2 \to \infty$ shows localized dynamics for typical initial states.

Conclusion. In summary, we studied the spinless extended Fermi-Hubbard chain in various limits of strong repulsion; the presence of any next-nearest-neighbor interactions breaks integrability. The model exhibits Hilbert space fragmentation for only nearest- or next-nearest-neighbor interactions as well as for both interaction terms combined. We derived effective hopping rules and construct frozen states, allowing us to derive lower bounds for the number of the highly localized frozen states and the dimension of the largest Hilbert space block. In contrast to the nonextended Fermi-Hubbard model, our results suggest that the extended model features interaction-induced localization. To substantiate these findings, we presented classical Markov simulations and indeed found localization provided that the density of initial movers is sufficiently low. While all our results have been derived for the fermionic model, due to its close relationship to the hard-core boson variant [45–47], the spin-1/2 XXZ chain [48,49], and the six-vertex model [50] we expect our results apply to a large class of systems.

Acknowledgments. We thank D. Mikhail for discussions and help with evaluating $\mathcal{D}_{\text{frozen}}$ and $\mathcal{D}_{\max}$ for large L. S.R. acknowledges support from the ARC through Grant No. FT180100211. L.H. gratefully acknowledges support from the Alexander von Humboldt Foundation.

[1] D. M. Basko, I. L. Aleiner, and B. L. Altshuler, Possible experimental manifestations of the many-body localization, Phys. Rev. B **76**, 052203 (2007).

[2] M. Schreiber, S. S. Hodgman, P. Bordia, H. P. Lüschen, M. H. Fischer, R. Vosk, E. Altman, U. Schneider, and I. Bloch, Observation of many-body localization of interacting fermions in a quasirandom optical lattice, Science **349**, 842 (2015).

[3] J. Smith, A. Lee, P. Richerme, B. Neyenhuis, P. W. Hess, P. Hauke, M. Heyl, D. A. Huse, and C. Monroe, Many-body localization in a quantum simulator with programmable random disorder, Nat. Phys. **12**, 907 (2016).

[4] J. Zhang, P. W. Hess, A. Kyprianidis, P. Becker, A. Lee, J. Smith, G. Pagano, I.-D. Potirniche, A. C. Potter, A. Vishwanath, N. Y. Yao, and C. Monroe, Observation of a discrete time crystal, Nature (London) **543**, 217 (2017).

[5] G. Kucsko, S. Choi, J. Choi, P. C. Maurer, H. Zhou, R. Landig, H. Sumiya, S. Onoda, J. Isoya, F. Jelezko, E. Demler, N. Y. Yao, and M. D. Lukin, Critical Thermalization of a Disordered Dipolar Spin System in Diamond, Phys. Rev. Lett. **121**, 023601 (2018).

[6] A. Smith, M. S. Kim, F. Pollmann, and J. Knolle, Simulating quantum many-body dynamics on a current digital quantum computer, npj Quantum Inf. **5**, 106 (2019).

[7] A. Kyprianidis, F. Machado, W. Morong, P. Becker, K. S. Collins, D. V. Else, L. Feng, P. W. Hess, C. Nayak, G. Pagano, N. Y. Yao, and C. Monroe, Observation of a prethermal discrete time crystal, Science **372**, 1192 (2021).

[8] X. Mi, C. Quintana, A. Greene, Z. Chen, J. Gross, F. Arute, K. Arya, J. Atalaya, R. Babbush, J. C. Bardin, J. Basso, A. Bengtsson, A. Bilmes, A. Bourassa, L. Brill, M. Broughton, B. B. Buckley, D. A. Buell, B. Burkett, N. Bushnell *et al.*, Time-crystalline eigenstate order on a quantum processor, Nature (London) **601**, 531 (2022).

[9] P. Frey and S. Rachel, Realization of a discrete time crystal on 57 qubits of a quantum computer, Sci. Adv. **8**, eabm7652 (2022).

[10] R. Nandkishore and D. A. Huse, Many-body localization and thermalization in quantum statistical mechanics, Annu. Rev. Condens. Matter Phys. **6**, 15 (2015).

[11] A. Pal and D. A. Huse, Many-body localization phase transition, Phys. Rev. B **82**, 174411 (2010).

[12] F. Wilczek, Quantum Time Crystals, Phys. Rev. Lett. **109**, 160401 (2012).

[13] D. A. Huse, R. Nandkishore, V. Oganesyan, A. Pal, and S. L. Sondhi, Localization-protected quantum order, Phys. Rev. B **88**, 014206 (2013).

[14] D. A. Abanin, E. Altman, I. Bloch, and M. Serbyn, Colloquium: Many-body localization, thermalization, and entanglement, Rev. Mod. Phys. **91**, 021001 (2019).

[15] N. Y. Yao, A. C. Potter, I.-D. Potirniche, and A. Vishwanath, Discrete Time Crystals: Rigidity, Criticality, and Realizations, Phys. Rev. Lett. **118**, 030401 (2017).

[16] C. W. von Keyserlingk, V. Khemani, and S. L. Sondhi, Absolute stability and spatiotemporal long-range order in Floquet systems, Phys. Rev. B **94**, 085112 (2016).

[17] M. Srednicki, Chaos and quantum thermalization, Phys. Rev. E **50**, 888 (1994).

[18] V. Khemani, A. Lazarides, R. Moessner, and S. L. Sondhi, Phase Structure of Driven Quantum Systems, Phys. Rev. Lett. **116**, 250401 (2016).

[19] J. M. Deutsch, Quantum statistical mechanics in a closed system, Phys. Rev. A **43**, 2046 (1991).

[20] M. Rigol, V. Dunjko, and M. Olshanii, Thermalization and its mechanism for generic isolated quantum systems, Nature (London) **452**, 854 (2008).

[21] V. Oganesyan and D. A. Huse, Localization of interacting fermions at high temperature, Phys. Rev. B **75**, 155111 (2007).

[22] F. Alet and N. Laflorencie, Many-body localization: An introduction and selected topics, C. R. Phys. **19**, 498 (2018).

[23] D. J. Luitz, N. Laflorencie, and F. Alet, Many-body localization edge in the random-field Heisenberg chain, Phys. Rev. B **91**, 081103(R) (2015).

[24] J. A. Kjäll, J. H. Bardarson, and F. Pollmann, Many-Body Localization in a Disordered Quantum Ising Chain, Phys. Rev. Lett. **113**, 107204 (2014).

[25] E. Altman and R. Vosk, Universal dynamics and renormalization in many-body-localized systems, Annu. Rev. Condens. Matter Phys. **6**, 383 (2015).

[26] E. V. H. Doggen, F. Schindler, K. S. Tikhonov, A. D. Mirlin, T. Neupert, D. G. Polyakov, and I. V. Gornyi, Many-body localization and delocalization in large quantum chains, Phys. Rev. B **98**, 174202 (2018).

[27] H. Bernien, S. Schwartz, A. Keesling, H. Levine, A. Omran, H. Pichler, S. Choi, A. S. Zibrov, M. Endres, M. Greiner, V. Vuletic, and M. D. Lukin, Probing many-body dynamics on a 51-atom quantum simulator, Nature (London) **551**, 579 (2017).

[28] S. Moudgalya, S. Rachel, B. A. Bernevig, and N. Regnault, Exact excited states of nonintegrable models, Phys. Rev. B **98**, 235155 (2018).

[29] S. Moudgalya, N. Regnault, and B. A. Bernevig, Entanglement of exact excited states of Affleck-Kennedy-Lieb-Tasaki models: Exact results, many-body scars, and violation of the strong eigenstate thermalization hypothesis, Phys. Rev. B **98**, 235156 (2018).

[30] C. J. Turner, A. A. Michailidis, D. A. Abanin, M. Serbyn, and Z. Papic, Weak ergodicity breaking from quantum many-body scars, Nat. Phys. **14**, 745 (2018).

[31] T. Iadecola and M. Žnidarič, Exact Localized and Ballistic Eigenstates in Disordered Chaotic Spin Ladders and the Fermi-Hubbard Model, Phys. Rev. Lett. **123**, 036403 (2019).

[32] C.-J. Lin and O. I. Motrunich, Exact Quantum Many-Body Scar States in the Rydberg-Blockaded Atom Chain, Phys. Rev. Lett. **122**, 173401 (2019).

[33] M. Serbyn, D. A. Abanin, and Z. Papic, Quantum many-body scars and weak breaking of ergodicity, Nat. Phys. **17**, 675 (2021).

[34] S. Moudgalya, B. A. Bernevig, and N. Regnault, Quantum many-body scars and Hilbert space fragmentation: A review of exact results, Rep. Prog. Phys. **85**, 086501 (2022).

[35] A. Morningstar, V. Khemani, and D. A. Huse, Kinetically constrained freezing transition in a dipole-conserving system, Phys. Rev. B **101**, 214205 (2020).

[36] S. Moudgalya and O. I. Motrunich, Hilbert Space Fragmentation and Commutant Algebras, Phys. Rev. X **12**, 011050 (2022).

[37] S. Moudgalya, A. Prem, R. Nandkishore, N. Regnault, and B. A. Bernevig, Thermalization and its absence within Krylov subspaces of a constrained hamiltonian, in *Memorial Volume for Shoucheng Zhang* (World Scientific, Singapore, 2021), pp. 147–209.

[38] P. Sala, T. Rakovszky, R. Verresen, M. Knap, and F. Pollmann, Ergodicity Breaking Arising from Hilbert Space Fragmentation in Dipole-Conserving Hamiltonians, Phys. Rev. X **10**, 011047 (2020).

[39] H. Zhao, A. Smith, F. Mintert, and J. Knolle, Orthogonal Quantum Many-Body Scars, Phys. Rev. Lett. **127**, 150601 (2021).

[40] V. Khemani, M. Hermele, and R. Nandkishore, Localization from Hilbert space shattering: From theory to physical realizations, Phys. Rev. B **101**, 174204 (2020).

[41] S. Pai, M. Pretko, and R. M. Nandkishore, Localization in Fractonic Random Circuits, Phys. Rev. X **9**, 021003 (2019).

[42] C. M. Langlett and S. Xu, Hilbert space fragmentation and exact scars of generalized Fredkin spin chains, Phys. Rev. B **103**, L220304 (2021).

[43] R. G. Dias, Exact solution of the strong coupling t-V model with twisted boundary conditions, Phys. Rev. B **62**, 7791 (2000).

[44] G. De Tomasi, D. Hetterich, P. Sala, and F. Pollmann, Dynamics of strongly interacting systems: From Fock-space fragmentation to many-body localization, Phys. Rev. B **100**, 214313 (2019).

[45] M. A. Cazalilla, R. Citro, T. Giamarchi, E. Orignac, and M. Rigol, One dimensional bosons: From condensed matter systems to ultracold gases, Rev. Mod. Phys. **83**, 1405 (2011).

[46] T. LeBlond, D. Sels, A. Polkovnikov, and M. Rigol, Universality in the onset of quantum chaos in many-body systems, Phys. Rev. B **104**, L201117 (2021).

[47] E. Bianchi, L. Hackl, M. Kieburg, M. Rigol, and L. Vidmar, Volume-Law Entanglement Entropy of Typical Pure Quantum States, PRX Quantum **3**, 030201 (2022).

[48] R. Orbach, Linear antiferromagnetic chain with anisotropic coupling, Phys. Rev. **112**, 309 (1958).

[49] L. Walker, Antiferromagnetic linear chain, Phys. Rev. **116**, 1089 (1959).

[50] E. H. Lieb, Residual entropy of square ice, Phys. Rev. **162**, 162 (1967).

[51] Here, we assume that we take the limits V_1 and V_2 *independently* to define the Hamiltonian $\hat{H}^{(3)}_{\infty}$. If we took the limit $V \to \infty$ with $V_1 = \alpha V$ and $V_2 = \beta V$, we would project onto the eigenspaces of $\sum_x (\alpha \hat{n}_x \hat{n}_{x+1} + \beta \hat{n}_x \hat{n}_{x+2})$.

[52] See Supplemental Material at http://link.aps.org/supplemental/10.1103/PhysRevB.106.L220301 for our derivations of A. Dimension of symmetry sectors, B. Spin/mover picture and periodic boundary conditions, C. Combinatorics of sector dimensions and D. Markov simulation and E. Overlap of active regions.